small methods
www.small-methods.com

# Tailoring the Structure of Low-Dimensional Halide Perovskite through a Room Temperature Solution Process: Role of Ligands

*Young-Taek Yoo, Do Yeon Heo, Sa-Rang Bae, Jinwoo Park, Tae-Woo Lee, Ho Won Jang,* Sang Hyun Ahn,* and Soo Young Kim**

**In this study, halide perovskite nanocrystals are synthesized by controlling the ligand length and amount, and investigated the effects on the change in the ligand length and amount on the shape, size, crystal structure, and optical properties of the perovskite nanocrystals. The results reveal the tendency and respective effects of amine and acid ligands on perovskite nanocrystals. The amine ligands bind directly to the perovskite nanocrystals. Consequently, the amine ligands with longer chains interfere with the aggregation of the initially formed nanocrystals, thus limiting the size of the halide perovskite nanocrystals. Similar to the amine ligands, the acid ligands directly bond with the perovskite nanocrystals; however, they are also indirectly distributed around the nanocrystals, thus affecting their structure and dispersion. Consequently, the acid ligands affect the assembly of the initially formed nanocrystals, which determine the shape and crystal structure of the nanocrystals. It is believed that the report will provide useful insight on the synthesis of halide perovskites for application in optoelectronic devices.**

## 1. Introduction

In recent years, all-inorganic cesium lead halide perovskites ($CsPbX_3$, X = Cl, Br, I, or combinations thereof) have attracted considerable attention for photonic and optoelectronic applications because of their outstanding optoelectronic properties, such as, high photoluminescence quantum yield (PLQY),[1] narrow emission spectrum for high color purity, high carrier mobility,[2] easily tunable optical absorption range,[3,4] simple fabrication via solution process, low material cost, and high defect tolerance.[5] In addition, $CsPbX_3$ has attracted significant research interest for application in various devices such as solar cells, light emitting diodes, photodetectors, and lasers. Schmidt et al. pioneered the synthesis of organic lead halide perovskite nanocrystals through a nontemplate synthesis method,[6] and consequently, a considerable amount of research has been conducted on the synthesis of perovskite nanocrystals. Various methods have been reported for the synthesis of halide perovskite nanocrystals including the hot injection method,[7] ligand-assisted reprecipitation (LARP) method,[8] template,[9] microwave,[10,11] sonication,[12–14] and the ball milling-assisted growth.[15] Among these methods, the hot injection method and the LARP method have attracted significant attention for the synthesis of perovskite nanocrystals. Protesescu et al. first introduced the hot injection method for the synthesis of highly luminescent colloidal $CsPbX_3$ NCs (X = Cl, Br, I, and mixed Cl/Br and Br/I systems), which exhibited bright (QY = 50–90%), stable, spectrally narrow, and broadly tunable photoluminescence (PL).[7] Subsequently, Feng Zhang et al.

Y.-T. Yoo, Prof. S. H. Ahn
School of Chemical Engineering and Materials Science
Chung-Ang University
Seoul 06974, Republic of Korea
E-mail: shahn@cau.ac.kr

D. Y. Heo, S.-R. Bae, Prof. S. Y. Kim
Department of Materials Science and Engineering
Institute of Green Manufacturing Technology
Korea University
Seoul 02841, Republic of Korea
E-mail: sooyoungkim@korea.ac.kr

J. Park
Department of Materials Science and Engineering
Seoul National University
Seoul 08826, Republic of Korea

Prof. T.-W. Lee
Department of Materials Science and Engineering
Institute of Engineering Research
Research Institute of Advanced Materials
Nano Systems Institute (NSI)
Seoul National University
Seoul 08826, Republic of Korea

Prof. T.-W. Lee
School of Chemical and Biological Engineering
Seoul National University
Seoul 08826, Republic of Korea

Prof. H. W. Jang
Department of Materials Science and Engineering
Research Institute of Advanced Materials
Seoul National University
Seoul 08826, Republic of Korea
E-mail: hwjang@snu.ac.kr

The ORCID identification number(s) for the author(s) of this article can be found under https://doi.org/10.1002/smtd.202100054.

**DOI: 10.1002/smtd.202100054**

 

developed a simple and versatile LARP technique for the fabrication of brightly luminescent colloidal $CH_3NH_3PbX_3$ quantum dots (QDs) with absolute PLQYs of 50–70%.[8]

Several studies have employed these known methods to synthesize perovskite nanocrystals with various shapes and sizes. An important aspect of nanotechnology is the control of the properties of materials when they take specific forms such as 1D or 2D nanostructures because of anisotropy. In addition, the performances of devices can be improved by employing nanomaterials that are specific to a particular device. For example, the nanowire structure can be employed to improve the performance of photodetectors.[16] In addition, the 1D microwires and 2D microplates of lead bromide perovskite can be used to achieve low-threshold two-photon pumped lasing owing to their large two-photon emission efficiency.[17] Consequently, the control of the morphological dimensionality of perovskite nanocrystals has attracted significant interest in modern nanochemistry.

Various studies have been conducted on the control of the molecular and morphological dimensionalities of perovskite crystals. The 0D, 1D, and 2D in the molecular dimensionality concept of perovskite crystals are completely different from nanodots (0D)-, nanowires (1D)-, and nanoplatelets(2D)- shaped nanocrystals based on 3D $ABX_3$.[18] The molecular dimensionality of perovskite crystal is determined by the spatial arrangement of the octahedral metal halide $BX_6$ units and has been found to have a notable effect on the stability[19,20] and PL mechanism[21–23] of perovskite crystals. Therefore, it is important to control the molecular dimensionality of perovskite nanocrystals, and several studies have been conducted to control this molecular dimensionality.

To synthesize various halide perovskite nanocrystals, tremendous efforts have been devoted to control the experimental conditions of previously reported synthesis method. Typically, the controllable variables during the synthesis of perovskite nanocrystals include the synthesis temperature, polarity of the antisolvent, reaction time, type, and amount of the surface ligands. Particularly, it is important to understand the effect of surface ligands on perovskite nanocrystals. Regardless of the method employed for the synthesis of perovskites, surface ligands are essential for the synthesis of colloidal perovskite nanocrystals. Carboxylic acids and amines are commonly used surface ligand precursors for the conventional synthesis of colloidal QDs. Furthermore, carboxylic acids and amines with long chains are commonly used as precursors for the synthesis of perovskite nanocrystal, with oleic acid and oleylamine being the most common. Generally, carboxylic acids and amines are used to facilitate the dissolution of inorganic precursors in solvent and to passivate perovskite nanocrystals by being present as ligands on the surface of the nanocrystal, thus stabilizing the colloidal perovskite nanocrystals.[24] In addition, they affect the shape and structure of nanocrystals by changing the kinetic pathway of the crystals that aggregate when the nanocrystals are formed.[25] However, to control the morphological dimensionality and molecular dimensionality of perovskite nanocrystals, it is important to extensively understand the role of surface ligands during the synthesis of perovskite nanocrystal. Several studies have been carried out to understand the effect on the ligand length and amount on the perovskite nanocrystals. For example, Sun et al. synthesized various perovskite nanocrystals using a combination of acid and amine ligands of various lengths: 0D spherical QDs, nanocubes, 1D nanorods, and 2D few-unit-cell thick nanoplatelets.[26] Aizhao Pan et al. revealed that the variation in the chain length of carboxylic acids and amines and temperature have no significant effect on the size and shape of nanocrystals.[27] In addition, a previous study synthesized a series of nanoscale lead (II) bromide perovskites with well-defined 2D, 3D, and quasi-2D layered structures using different amounts of organic ammonium bromide.[28]

However, the effect of the length or amount of carboxylic acid and amine ligands on the shape, size, and structure of the halide perovskite nanocrystals during the synthesis is unclear. Herein, we investigated the effect of carboxylic acids and amines on the size, shape, and crystal structure of perovskite nanocrystals. The perovskite nanocrystals were synthesized by varying the length of the acid and amine ligands using a ligand-assisted room-temperature reprecipitation strategy, a well-known perovskite nanocrystal synthesis method. To verify the role of the acid and amine ligands, perovskite nanocrystals were synthesized while fixing the length of one of the acid and amine ligands and changing the length of the other. Subsequently, the role of the acid and amine ligands was identified by examining the trends in the changes in the shape, size, and crystal structure of the perovskite nanocrystals. In addition, to determine the reason for the effects of the acid and amine ligands, the mechanism of the ligand binding was examined by varying the amounts of the acid and amine ligands and investigating the binding of the ligands on the nanocrystalline surfaces of the perovskite.

## 2. Results and Discussion

In this study, the perovskite nanocrystals were synthesized by the recrystallization method. First, precursors including $PbBr_2$, Cs-oleate, and a combination of various organic acids and amines were dissolved in dimethylformamide (DMF), a good solvent. Subsequently, the as-prepared solution was quickly added to toluene, a poor solvent, to induce recrystallization, and the resulting nanocrystals were separated through a centrifugation process. The obtained nanocrystals were washed with hexane and ethyl acetate and finally dispersed in hexane, and named A*n*B*n*'-NCs, where *n* is the number of carbon atoms in the carboxylic acid and n' is the number of carbon atoms in the amine. The synthesized A*n*B*n*'-NCs are summarized in Table S1, Supporting Information. The carboxylic acids used in this study include acetic acid, hexanoic acid, octanoic acid, decanoic acid, and oleic acid, where *n* can be 2, 6, 8, 10, and 18. In addition, four amines were used in this study including butylamine, octylamine, dodecylamine, and oleylamine, and *n*' can be 4, 8, 12, 18. The details of the synthesis process can be found in Section 4.

First, perovskite nanocrystals were synthesized by fixing the length of butylamine and changing the chain length of the acid ligands. The shape of the synthesized perovskite nanocrystals was investigated by field-emission scanning electron microscopy (FE-SEM). When acetic acid was used as the acid ligand, nanobelt-type nanocrystals were observed; however,

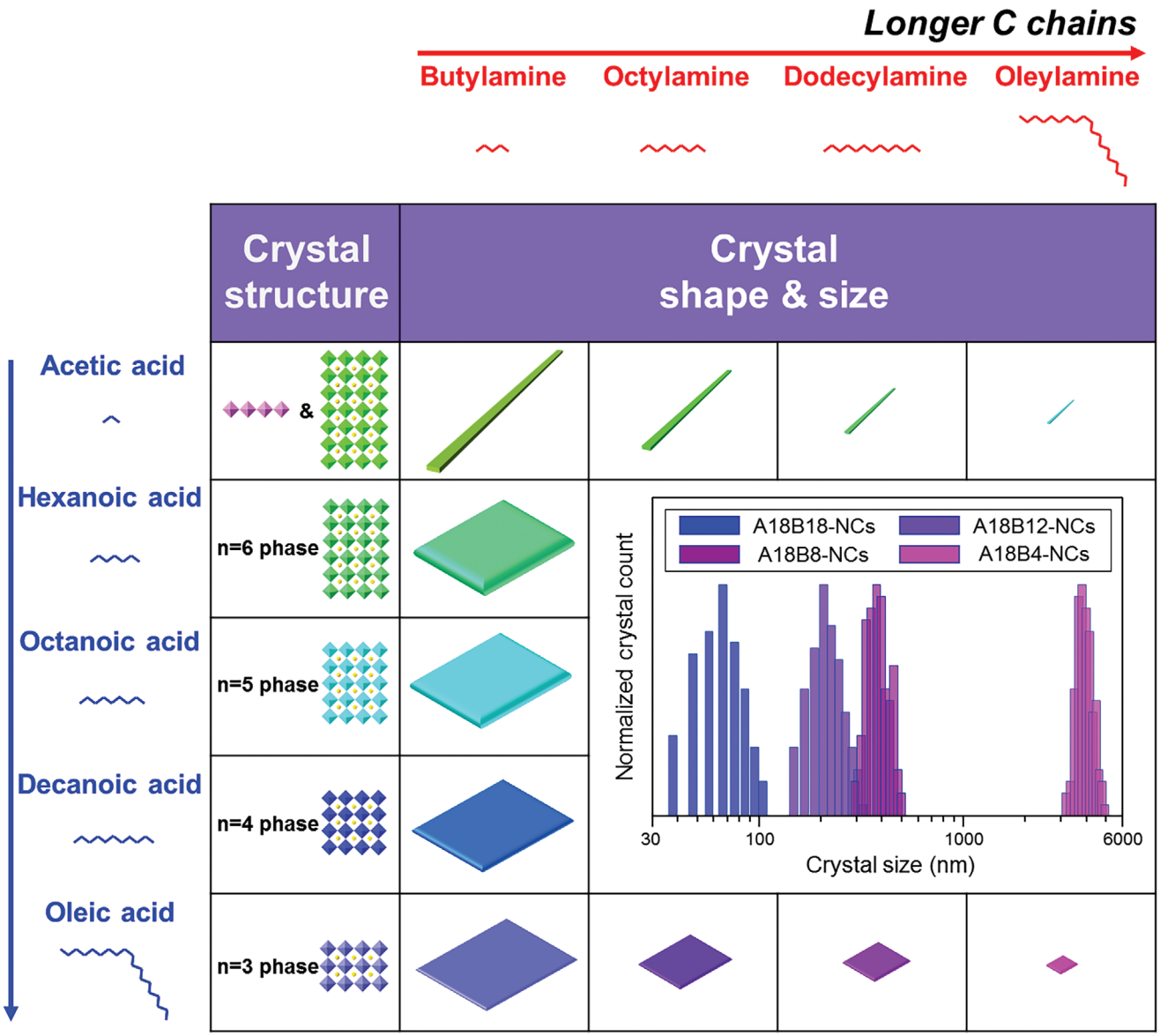


**Figure 1.** Schematic illustration of the change in shape, crystal structure, and size of the $CsPbBr_3$ perovskite nanocrystals as a function of the chain length of the carboxylic acid and amine.

nanoplatelet-shaped nanocrystals were observed when other acids were used. As the identified nanocrystals were largely in the form of nanobelts and nanoplatelets, experiments on the change in the length of the amine ligands were carried out for both cases (nanobelt and nanoplatelet) using acetic acid and oleic acid as the acid ligands. **Figure 1** shows a schematic illustration of our results. With a change in the length of the acid ligand, the shape and crystal structure of the perovskite crystals, rather than the size, changed. In addition, with an increase in the length of the amine ligand, the size of the perovskite crystals decreased; however, their shape was maintained.

**Figure 2** shows the changes in shape, crystal structure, and optical properties of the nanocrystals when butylamine (B4) was used as the amine ligand and the acid ligand length was changed. Figure 2a shows the changes in the shape of the nanocrystals with an increase in the length of the acid ligand. The A2B4-NCs, in which acetic acid was used, exhibited a nanobelt shape with a length of 10–20 µm and width of 200 nm. When acids other than acetic acid were used, nanoplatelet-shaped nanocrystals were mostly observed, and the width of the nanoplatelets was approximately 5 µm. In addition, when octanoic acid (A8) and decanoic acid (A10) were used, other forms of nanocrystals were observed in addition to the nanoplatelets. In the case of octanoic acid, nanorod-shaped nanocrystals with a length of 1 µm were observed, as shown in Figure S1a, Supporting Information. When decanoic acid was used, nanodot-shaped nanocrystals with a radius of 50 nm were observed, as shown in Figure S1b, Supporting Information. In addition, the shape of the nanocrystals changed with a change in the length of the acid. X-ray diffraction (XRD) measurements were performed to determine any change in the crystal structure of the perovskites. As shown in Figure 2b, the XRD peak changed

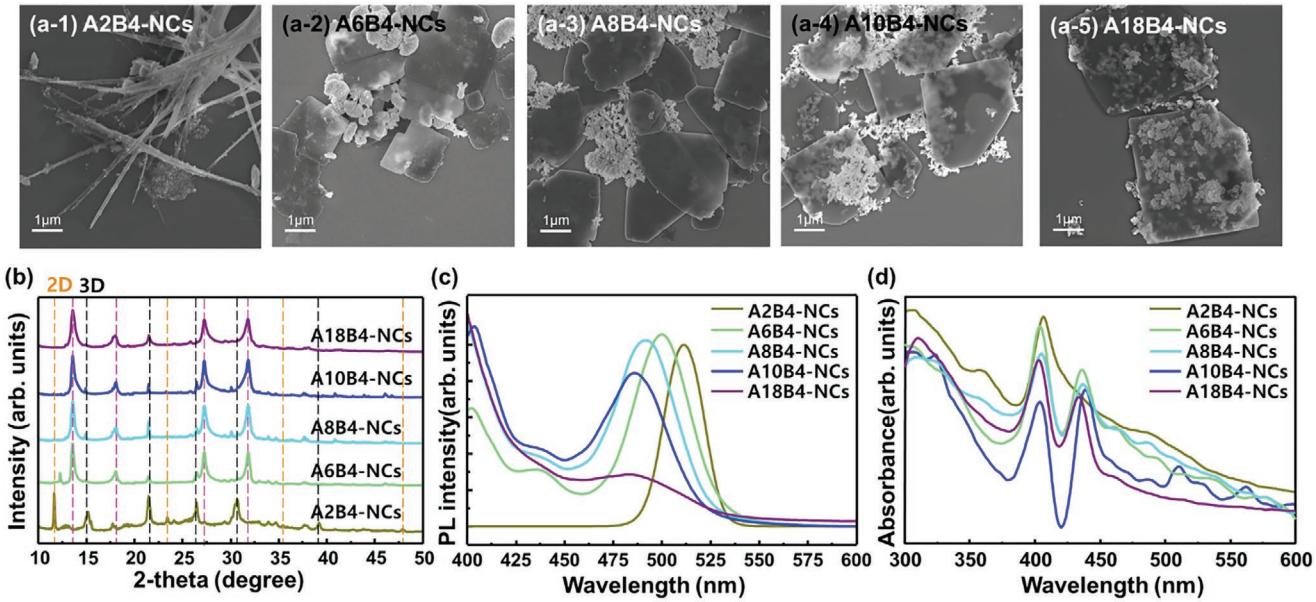


**Figure 2.** Characterizations of the $CsPbBr_3$ perovskite nanocrystals as a function of the length of the acid ligand. a) FE-SEM images of the AnB4-NCs synthesized using carboxylic acids with various length and butylamines as the ligands. b) XRD patterns of AnB4-NCs with changes in the acid ligand length. XRD patterns of the 2D ($n = 1$) phase (orange vertical lines), 3D ($n = \infty$) phase (black vertical lines), and quasi-2D ($n = 3$) phase (pink vertical lines) are labeled. c) PL emission and d) optical absorption spectra of the AnB4-NCs synthesized by changing the length of the acid ligands.

with a change in the length of the acid ligand. In addition, the XRD patterns of the A2B4-NCs exhibited peaks corresponding to 3D and 2D perovskite structures. These peaks were observed as a complex in which two structures existed together in one nanocrystal, rather than a mixture in which the nanocrystals of 3D perovskite structure and nanocrystals of 2D perovskite structure were individually present. When the nanocrystals were synthesized using acids other than acetic acid, new peaks (pink vertical lines) were observed at four $2\theta$ values (13.58, 18.07, 27.31, 31.86°), and no peaks corresponding to 3D and 2D perovskite structures were observed. These new peaks could be attributed to the quasi-2d perovskite structure because of the peak shifts in the PL and ultraviolet-visible (UV–vis) absorption spectra in Figure 2c,d. It is known that the diffraction peaks of the quasi-2d perovskite structure are different from those of the 3D and 2D perovskite structures.[28] Herein, the meaning of the new XRD were evaluated by calculations; the results are shown in Table S2, Supporting Information. The results confirmed that these diffraction peaks could be attributed to the quasi-2d perovskite structure, $n = 3$ phase. In addition, the positions of the new peaks were consistent with the positions of the peaks on the calculated $n = 3$ phase; however, the peaks of $n > 4$ compositions were not shown here because of their weak and small n-phase diffraction.[29]

The PL and UV–vis absorption spectra of the perovskites were measured to confirm the change in the optical properties of the perovskites with a change in the length of the acid ligands. The optical properties of the samples changed with an increase in the length of the acid ligand owing to the change in the perovskite crystal structure from the complex structure 3D and 2D perovskite structures to a quasi-2D perovskite structure. As shown in Figure 2c, rather than a narrow PL spectrum peak generally exhibited by 3D perovskite-structured nanocrystals, the nanoplatelet-shaped perovskite crystals exhibit uniquely shaped, wide PL spectra. Previous studies have reported that the peak position of qausi-2D perovskite nanocrystal in the PL spectrum is based on the number of the octahedral metal halide $BX_6$ unit cell layers, and each unit cell layer number exhibits a unique PL peak position because of the quantum-size effect. This indicates that the nanoplatelet-shaped perovskite crystals, which exhibited broad PL peaks at various wavelengths, were corrugated 2D structures rather than quasi-2D structures with uniform unit cell layers. This corrugated 2D structure could be attributed to the relatively large perovskite crystals, which restricted the formation of uniform unit cell layers. The maximum number of the unit cell layers of the perovskite crystals synthesized using acids of various chain lengths and butylamine based on the PL emission wavelength is as follows: The maximum number of unit cell layers in A2B4-NCs, A6B4-NCs, A8B4-NCs, A10B4-NCs, and A18B4-NCs were ∞, 6, 5, 4, and 3, respectively. With an increase in the length of the acid ligand, the maximum number of the unit cell layers decreased. As shown in Figure 2d, the UV–vis absorption spectra are consistent with the PL spectra. Additionally, secondary absorption peaks were observed at lower wavelengths when the nanocrystals were synthesized using acids except acetic acid, whereas A2B4-NCs exhibited only one UV absorption peak at 520 nm. These secondary absorption peaks could be attributed to quasi-2D excitonic absorption, indicating that the quasi-2d structure was dominant in the nanocrystals, which is because the 3D absorption peak decreased and the absorption peak corresponding to the quasi-2D structure increased.[30] Furthermore, the PL and optical absorption spectra revealed that the 3D and 2D perovskite crystal structures changed to a quasi-2D perovskite crystal structure with an increase in the length of the acid ligand, which is consistent with the XRD measurement. In

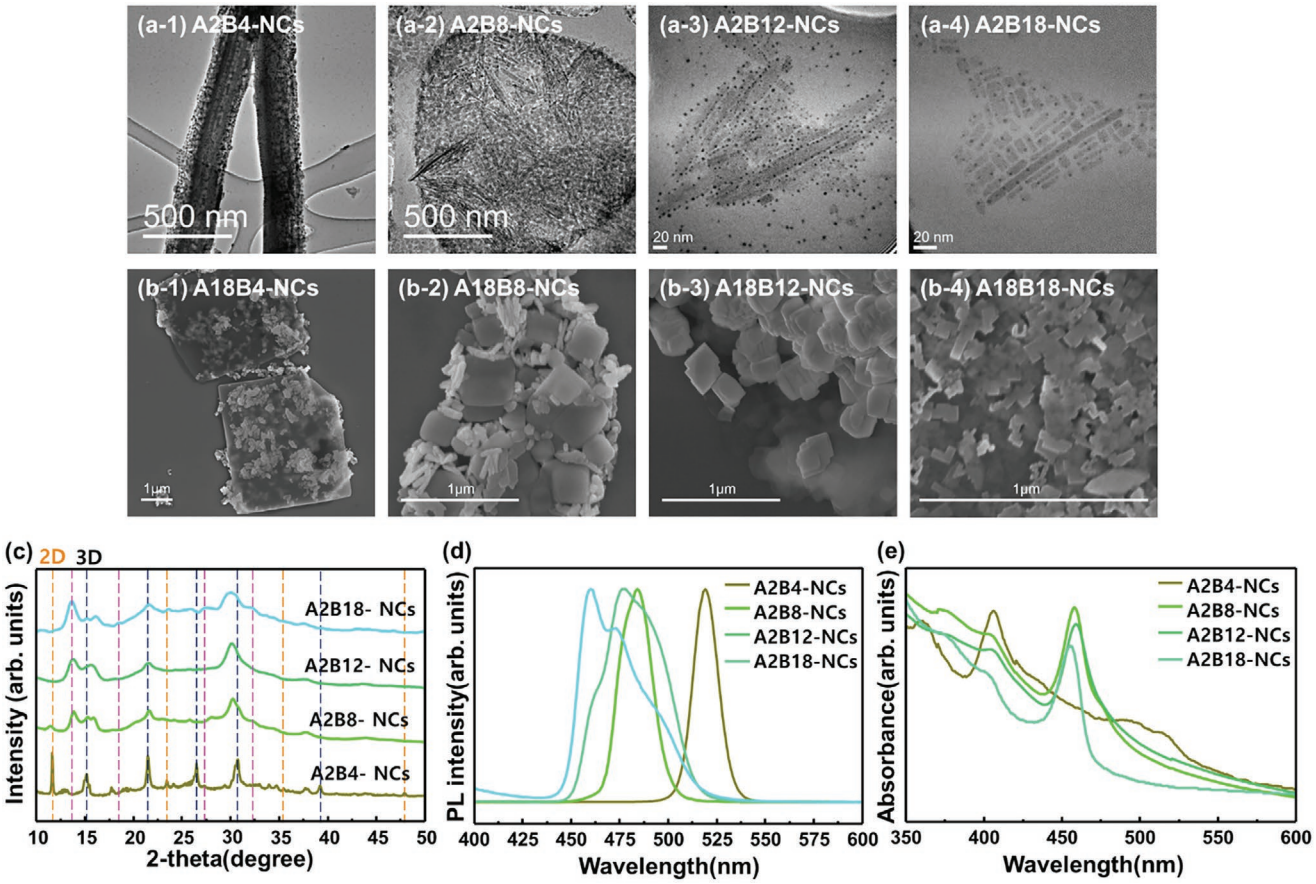


**Figure 3.** Characterizations of the $CsPbBr_3$ perovskite nanocrystals as a function of the length of the amine ligand. a) FE-SEM images of the A2Bn'-NCs synthesized using acetic acid and amines with various length as ligands. b) FE-SEM images of the A18Bn'-NCs synthesized using oleic acid and amines with various length as ligands. c) XRD patterns of the A2Bn'-NCs with changes in the amine ligand length. d) PL emission and e) optical absorption spectra of the A2Bn'-NCs synthesized with a change in the length of the amine ligands.

summary, the results shown in Figure 2 indicate that the acid ligand affects the shape and crystal structure of the perovskite nanocrystals.

In this study, with a change in the acid ligand length, the nanocrystals were synthesized in two major forms: Nanobelts and nanoplatelets. As shown in Figure S2a,b, Supporting Information, nanobelt-shaped crystals were formed when acetic acid (A2) was used. Therefore, experiments on the change in the length of the amine ligands were performed for both cases (nanobelt and nanoplatelet) using acetic acid and oleic acid as the acid ligands. Similar to the observation when the acid ligand length was changed, the shape and size of the nanocrystals changed with a change in the length of the amine ligand. As shown in **Figure 3**a, when nanocrystals were synthesized using acetic acid (A2) and butylamine (B4), large nanobelts with lengths is 10–20 μm and widths of 200 nm were formed. With an increase in the length of the amine ligand, the size of the nanocrystals gradually decreased, while maintaining the shape. When octylamine (B8) was used, nanobelts with a length of 500 nm were produced; nanobelts with a length of 150 nm were produced when dodecylamine (B12) was used; and nanobelts with a length of 20 nm were produced when oleylamine (B18) was used. A similar phenomenon was also observed when oleic acid was used as the acid ligand. As shown in Figure 3b, nanoplatelet-type nanocrystals with a length of 5 μm were observed when oleic acid (A18) and butylamine (B4) were used. In addition, with an increase in the length of the amine ligand, the size of the nanoplatelets decreased. When octylamine (B8) was used, nanoplatelets with a length of 300 nm were obtained; when dodecylamine (B12) was used, nanoplatelets of 100 nm length on one side were produced; and nanoplatelets below 50 nm were produced when oleylamine (B18) was used. Similar to when the length of the acid ligand was changed, XRD measurements were performed to examine the change in the crystal structure of the perovskites with a change in the amine length. Similar to when the acid ligan length was varied, the XRD peak position of the nanocrystals also changed with a change in the amine length. As shown in Figure 3c, A2B4-NCs can be identified as complexes of 3D and 2D perovskite structures. In addition, A2B8-NCs exhibited peaks corresponding to 3D and 2D perovskite structure complexes; however, additional peaks corresponding to quasi-2D structures were also observed and the intensity of the peak corresponding to the 2D perovskite structure reduced. In the XRD pattern of the A2B12-NCs, the 2D perovskite peak disappeared and the peak corresponding to the quasi-2D structure was closer to the peak corresponding to the $n = 3$ phase, which was also observed in the XRD pattern of A2B18-NCs. With a change in the length of the acid amine,

there were changes in the diffraction peaks of the crystals synthesized with various amines with different lengths; however, the cause of these changes was different. The change in the diffraction peak with a change in the amine length could be attributed to the size of the nanocrystals. For example, the size of the A2B4-NCs, which are large nanobelt-shaped crystals, decreased with an increase in the length of the amine ligand. Consequently, the thickness of the nanobelt reduced, resulting in a quasi-2D crystal structure.

Figure 3d,e show the PL and UV–vis absorption spectra of the perovskite nanocrystals, respectively, with a change in the amine length. With an increase in the amine length, the PL spectra were blue-shifted. In the perovskite nanocrystals with sizes larger than the Bohr diameter, $D_B$ (>10 nm), the PL emission wavelength was not sensitive to the crystal size of the PL owing to the crystal structure-based electronic band structures.[31] Therefore, the blueshift that appeared in the PL spectra could be attributed to the quasi-2D structure, which was caused by a decrease in the size of the nanocrystals with an increase in the length of the amine ligand, rather than to the size of the nanocrystals. These blueshifts were also observed in the UV–vis absorption spectra (Figure 3e). Compared to the corrugated 2D nanoplatelet synthesized using butylamine (B4) and acids other than acetic acid (A2), the nanocrystal exhibited a narrower PL emission peak. This indicates that a relatively uniform phase was produced with a decrease in the size of the nanocrystals. A similar phenomenon was also observed when the nanocrystals were synthesized with oleic acid (A18) and acetic acid. As shown in Figure S2c,d, Supporting Information, the PL emission peak and UV–vis absorption peak blue-shift with an increase in the amine length. The blue-shift in the PL emission peak could be attributed to the change in the number of the unit cell layers owing to the decrease in the thickness of the layers with a decrease in the size of the nanoplatelets. The A18B18-NCs with the smallest nanoplatelet size exhibited a narrow PL peak, indicating that a uniform phase was formed with a decrease in the size of the nanoplatelets. The PL peak wavelengths and the numbers of unit cell layers based on the perovskite types are summarized in Table S3, Supporting Information. In summary, the results in Figure 3 indicate that amine ligands directly affect the size of the perovskite nanocrystals, rather than the structure or shape of the nanocrystal.

Perovskites nanocrystals were synthesized by varying the amounts of amine ligands and acid ligands to understand the effect of the change in the length of the acid and amine ligands on the nanocrystals. The effects of the amount of ligands added during the perovskite nanocrystal synthesis were investigated only for A2B4-NCs, the perovskite nanocrystals synthesized using acetic acid and butylamine. As shown in the FE-SEM images in **Figure 4**a, the width of the nanobelt decreases with an increase in the amount of acid ligand. In addition, the effect of the ligand amounts on the degree of dispersion of the nanocrystals was investigated. When a low acetic acid content was added during synthesis, the nanocrystals agglomerated; the FE-SEM images also revealed that the nanocrystals agglomerated together. However, with an increase in the acetic acid content, individual, rather than agglomerated, nanobelts were observed in the FE-SEM images. This phenomenon can also be observed in the PL and UV–vis absorption spectra in Figure 4b,c. With a change in the length of the acid ligand, the positions of the PL and UV–vis absorption peaks remained constant. However, with an increase in the amount of the acid ligand, the full width at half maximum of the PL spectrum decreased. This could be attributed to an increase in the dispersion of the nanocrystals with an increase in the amount of acid ligand, as confirmed by the FE-SEM image. Moreover, as shown in Figure S3a, Supporting Information, the highest PLQY was 49.127 when 0.023 mL of acetic acid was added. It is important to set an appropriate amount of acid for stability of dispersion or PLQY. In addition, Fourier transform-infrared (FT-IR) spectroscopy was performed to confirm the presence of acid and amine ligands in the nanocrystal and to examine the change in the bonds on the surface of the nanocrystals with a change in the ligand amount. Figure 4d shows the FT-IR graph at the full wavelength, and Figure 4e shows the high-resolution graph of the FT-IR that zooms in on the main points. The presence of ligands can be confirmed by the presence of $COO^-$ stretching vibration peak from the carboxylic acid ligands at 1545 $cm^{-1}$ and the $N^+$—H bending vibration peak from the amine ligands at 1575 $cm^{-1}$. As shown in Figure 4e, with an increase in the amount of acetic acid added during synthesis, the intensity of the peak at 1575 $cm^{-1}$ corresponding to the amine ligands remained unchanged, while the intensity of the peak at 1545 $cm^{-1}$ corresponding to the acid ligands increased. With a further increase in the amount of acetic acid added during synthesis, the number of acid ligands distributed around the nanocrystals increased; however, this had no significant effect on the binding of the amine ligands.

The effect on a change in the amount of the amine ligands during the synthesis of the perovskite nanocrystals on the nanocrystals was also investigated using the A2B4-NCs. As shown in **Figure 5**a, there is no significant change in the shape of the nanocrystals with a change in the amount of amines; however, there was a slight change in the size of the crystals. As shown in Figure 5b,c, the PL spectrum and UV–vis absorption spectrum were measured to examine the optical properties of the nanocrystals as a function of the amount of amine. As shown in Figure 5c, with an increase in the amount of amine, the peak position of the PL spectrum slightly blue-shifts. However, the peak position of the UV absorption spectrum in all the four cases remained constant. The blue-shift in the PL spectrum could be attributed to the effect of surface defect passivation on the amount of amine. With an increase in the amount of amine, the defects on the surface of the nanocrystals were more passivated by the amine ligands, resulting in a smaller trap structure and the blue-shift of the PL. This result was also confirmed by measuring PLQY. As shown in Figure S3b, Supporting Information, samples with a higher amount of amine tended to show higher PLQY. This appears to be a result of reduced trap state emission due to surface passivation by amine. Figure 5d,e show the results of FT-IR measurement as a function of a change in the amine amount. Figure 5d is the graph at full wavelength, and Figure 5e is the high-resolution graph showing the enlarged part of the full wavelength that detected the presence of acid and amine ligands. As shown in Figure 5e, with an increase in the amount of amine, both the intensities of the peak at 1575 $cm^{-1}$, corresponding to $N^+$—H bending vibration, and the

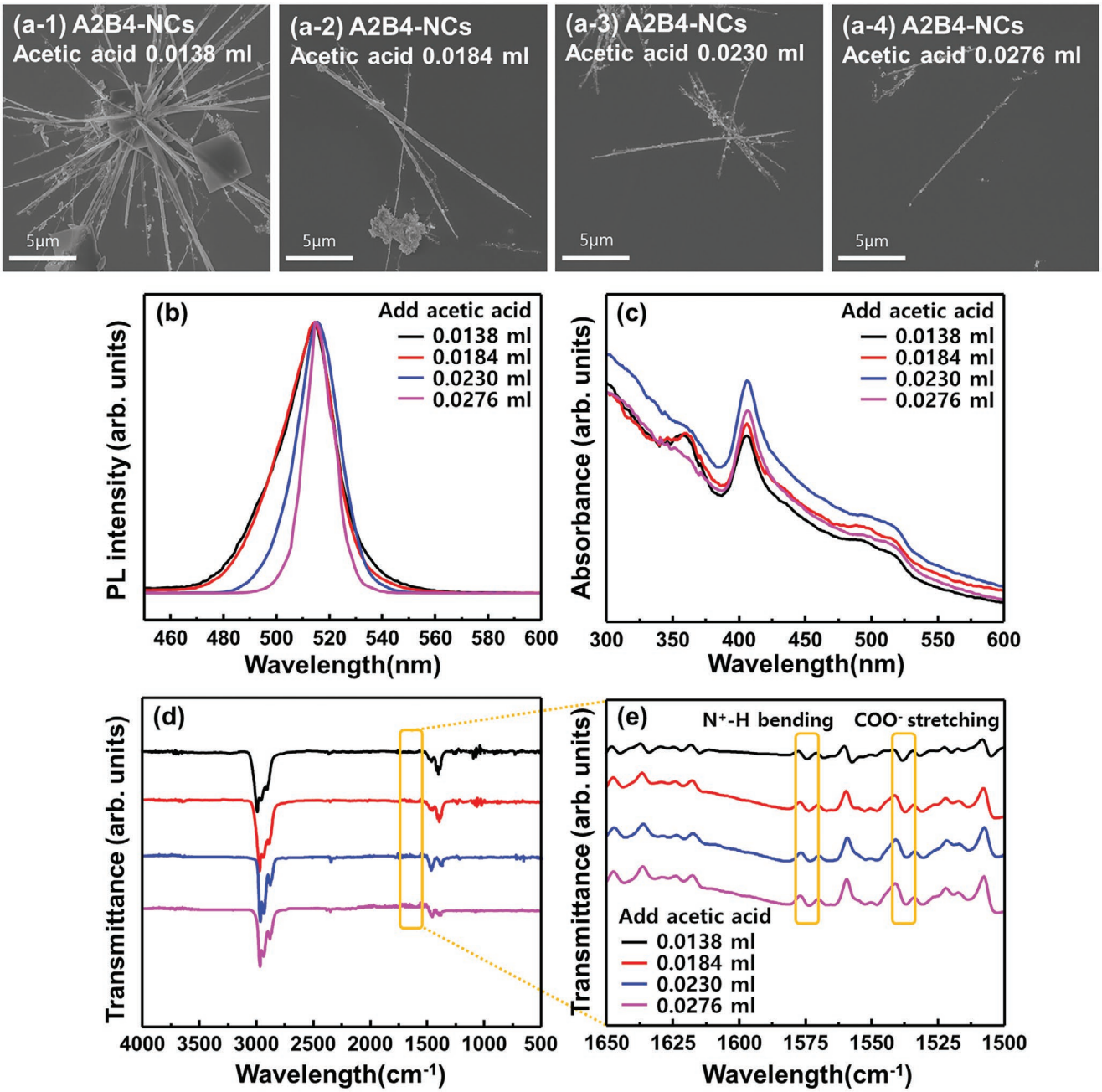


**Figure 4.** Characterizations of the A2B4-NCs synthesized using acetic acid and butylamine as a function of the amount of the acetic acid. a) FE-SEM images of various A2B4-NCs synthesized by changing the amount of acetic acid. b) PL emission, c) optical absorption, and d) FT-IR spectra of various A2B4-NCs synthesized by changing the amount of acetic acid. e) high-resolution FT-IR graph with an enlarged view of the yellow box of the FT-IR spectra in (d). $NH^+$ bending peaks and $COO^-$ stretching peaks are labeled with yellow boxes.

peak at 1545 $cm^{-1}$, corresponding to $COO^-$ stretching vibration, increased. This indicates that the amount of amine and acid ligands bound to the nanocrystals increased with an increase in the amount of amine, implying that more amine ligands bind to the nanocrystals with an increase in the amount of amine, resulting in an increase in the number of acid ligands binding to the nanocrystal. The change in the binding of the acid and amine ligands as a function of the amount of acid and amine added during synthesis indicates that the amine ligands were directly bonded to the nanocrystals and the acid ligands were directly bonded to the nanocrystal, but also indirectly through the amine ligands. The ligand binding mechanisms presented here are consistent with previously reported results and were confirmed using a different method.[32]

To further understand the ligand binding mechanisms, oleic acid and oleylamine were added to the A2B4-NCs dispersed in hexane after purification, and the nanocrystals were visually observed; and FE-SEM measurements were obtained as well.

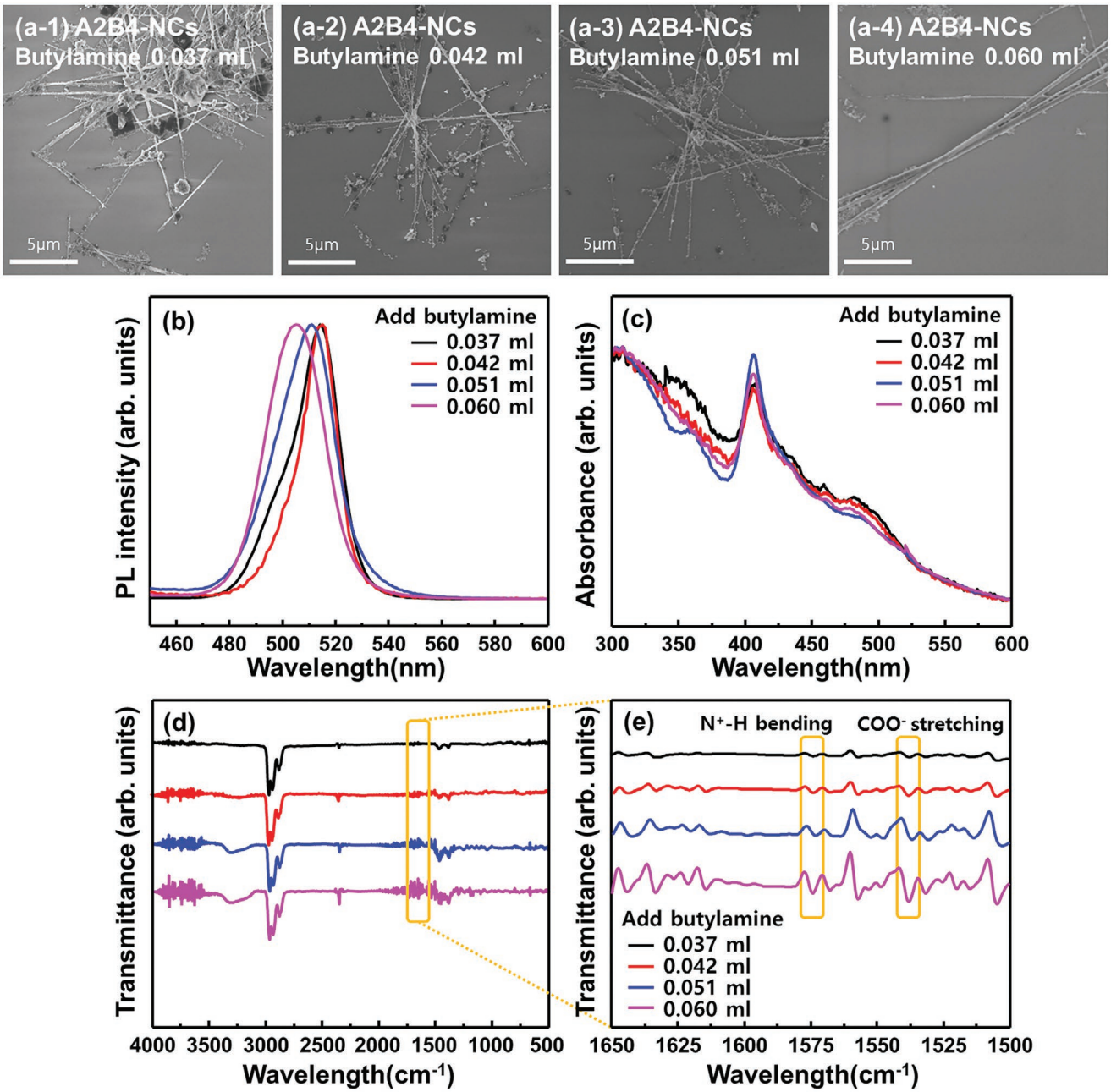


**Figure 5.** Characterizations of the A2B4-NCs synthesized using acetic acid and butylamine as a function of the amount of the butylamine. a) FE-SEM images of various A2B4-NCs synthesized by changing the amount of butylamine. b) PL emission, c) optical absorption, and d) FT-IR spectra of various A2B4-NCs synthesized by changing the amount of butylamine. e) high-resolution graph with an enlarged view of the yellow box of the FT-IR spectra (d). $NH^+$ bending peaks and $COO^-$ stretching peaks are labeled with yellow boxes.

**Figure 6**a shows the photographs of the A2B4-NCs dispersed in hexane and A2B4-NCs after the addition of oleic acid and oleylamine. As shown in Figure 6a, nanocrystals agglomerated with each other in hexane before oleic acid was added. However, with the addition of oleic acid, the dispersion of the nanocrystals in hexane increased. In contrast, when oleylamine was added instead of oleic acid, a completely different phenomenon appears. When oleylamine was added, the agglomerated crystals visible to the naked eye disappeared and appeared as if there was only a clear, light green solution. The crystals appeared to be cleaved by the additional oleylamine, as confirmed by the FE-SEM results. As shown in Figure 6b-1, the A2B4-NCs dispersed in untreated hexane are packed together in the form of nanobelts. Figure S4a,b, Supporting Information, shows FE-SEM images of A2B4-NCs with the addition of oleic acid and oleylamine without repurification. When oleic acid was added, the nanocrystals were observed in the form of nanobelts, but were well dispersed; thus, clusters were not observed. When oleylamine was added, the nanobelt-type crystals could not be identified and the crystals seemed broken. The nanocrystals

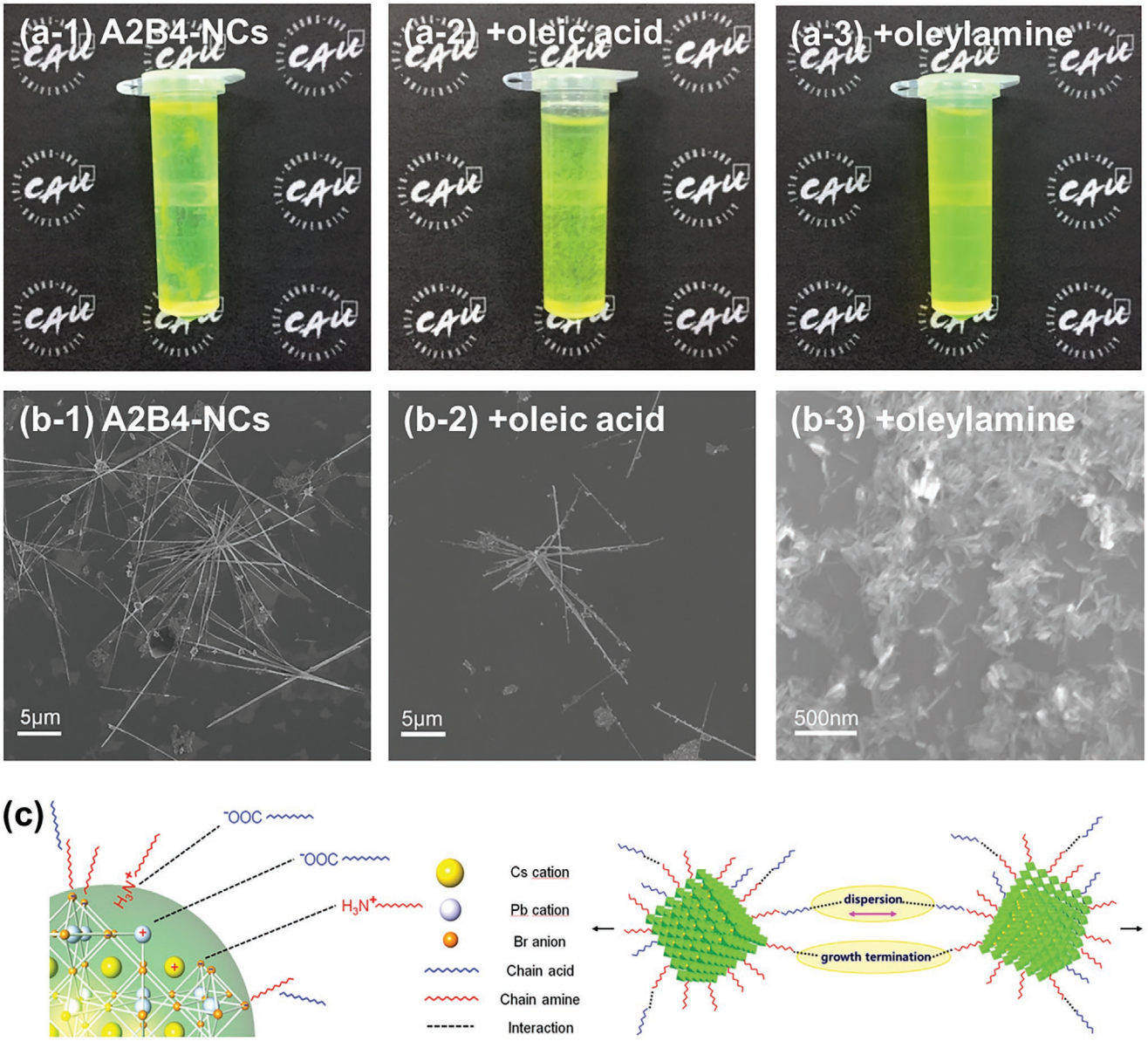


**Figure 6.** a) Photographs of the A2B4-NCs under different conditions. a-1) A2B4-NCs in hexane, a-2) +oleic acid, and a-3) +oleylamine are obtained by adding oleic acid and oleylamine to (a-1), respectively. b) FE-SEM images of the A2B4-NCs, +oleic acid, and +oleylamine after repurification. c) Schematic illustrations of the mechanism by which the acid and amine ligands bind to the perovskite nanocrystals and the respective role of the acid and amine ligands.

could not be observed because the amine did not dry well. Therefore, oleic acid and oleylamine were added respectively into A2B4-NCs, and the FE-SEM images were taken after repurification. As shown in Figure 6b-2, after the addition of oleic acid into the A2B4-NCs, 20 μm long nanobelts were observed; however, 500 nm long nanorods were observed after the addition of oleylamine into A2B4-NCs, which are smaller than those before the addition (Figure 6b-3). This indicates that oleic acid only affected the dispersion degree of the nanocrystal, and not the size, whereas, oleylamine affected the size and the nanobelt was split into nanorods with an increase in the amount of oleylamine added. The FT-IR spectra of A2B4-NCs with oleic acid and oleylamine are also shown in Figure S4c,d, Supporting Information. When oleic acid was added, only the binding of the acid ligand was increased, but when oleylamine was added, the binding energy of the anime and acid ligands increased, which is consistent with previous results.

These results confirm that the acid ligands indirectly bind to the nanocrystals through the amine ligands and are distributed in the outermost area of the nanocrystal, thus affecting the dispersion of the nanocrystal. In contrast, the amine ligands directly bind to the nanocrystals and affect their size. Figure 6c is a schematic illustration of the binding mechanism of the acids and amine ligands and the respective roles of the acids and amine ligands. During LARP synthesis, nanobelt- or nanoplatelet-shaped perovskite crystals are formed by the

agglomeration of the initial nanocrystals at the initial stage of reprecipitation, as shown in Figure S5, Supporting Information. Consequently, with an increase in the length of the amine ligands, the aggregation of the nanocrystals formed at the initial stage of crystal precipitation and termination of the growth of the nanocrystal decreased. This indicates that the amine ligands limited the size of the nanocrystals. In contrast, the acid ligands bound directly to the nanocrystals, but also indirectly to the nanocrystals through the amine ligands. Consequently, it was located at the outermost side of the nanocrystals and significantly influenced the dispersion of the nanocrystals. The influence on dispersion affected the aggregation of the initial crystals formed at the initial stages of crystallization, thus affecting the crystal structure and shape of the nanocrystals.

## 3. Conclusion

In summary, we demonstrated the respective roles of carboxylic acids and amines, which are essential for the synthesis of colloidal perovskite nanocrystals, as surface ligands during the synthesis of perovskite nanocrystals. Although previous studies have investigated the role of ligands in perovskite nanocrystals to some extent, the respective roles of carboxylic acids and amines are ambiguous. Therefore, in this study, we synthesized perovskite nanocrystals by fixing one of the carboxylic acids and amines and changing the length of the other and observing the changes in the perovskite nanocrystals, identifying the trend in the changes. The results revealed that a change in the length of the carboxylic acid used during the synthesis affected the shape and crystal structure of the perovskite nanocrystals, rather than the size. In contrast, a change in the amine length affected the size of the perovskite nanocrystals, as the size of the perovskite gradually decreased with an increase in the length of the amine ligand; however, the shape of the nanocrystals was maintained. The roles of carboxylic acids and amines can be determined by understanding how ligands bind to nanocrystals. After the analysis of the perovskite nanocrystals synthesized with varying amounts of either carboxylic acid or amine, the results revealed that the amine ligands bound directly to the perovskite nanocrystals, whereas the acid ligands directly bound to the perovskite nanocrystals, and also indirectly through the amine ligands. This indicates that the length of the amine ligands that directly bind to the nanocrystals limits the size of the nanocrystals, and acid ligands that indirectly bind to the nanocrystals affect the aggregation of the nanocrystals formed at the initial stage, thus affecting the crystal shape and crystal structure. The comprehensive understanding of the role of acid and amine ligands in the synthesis of perovskite nanocrystals will provide useful insights on the control of the morphological dimensionality and molecular dimensionality of perovskite nanocrystals.

## 4. Experimental Section

*Materials*: $Cs_2CO_3$ (Sigma-Aldrich, 99.9%), $PbBr_2$ (Sigma-Aldrich, ≥98%), 1-octadecene (ODE, Sigma-Aldrich, 90%), *N*,*N*-dimethylformamide (DMF, Daejung, ≥99.5%), acetic acid (Sigma-Aldrich, ≥99.9%), hexanoic acid (Sigma-Aldrich, ≥99.5%), octanoic acid (Sigma-Aldrich, 98%), decanoic acid (Sigma-Aldrich, ≥98%), oleic acid (Alfa Aesar, tech, 90%), butylamine (Sigma-Aldrich, 99.5%), octylamine (Sigma-Aldrich, 99.9%), dodecylamine (Sigma-Aldrich, 98%), oleylamine (Sigma-Aldrich, technical grade, 70%), toluene (Daejung, 99.5%), hexane (Daejung, ≥96%), and ethyl acetate (Alfa Aesar, 99%) were purchased and used as received without further purification.

*Preparation of Cs-oleate Solution*: Briefly, 0.814 g $Cs_2CO_3$ (Sigma-Aldrich, 99.9%) was placed in a 100 mL 3-neck flask with 10 mL ODE (Sigma-Aldrich, 90%) and 2.5 mL oleic acid (OA, Alfa Aesar, tech 90%), and the solution was dried for 1 h at 120 °C. After drying, the mixture was heated to 150 °C under $N_2$ to enable the reaction of $Cs_2CO_3$ with OA. Heating was stopped when no precipitate was observed in the mixed solution, indicating the completion of the reaction. Because cs-oleate is precipitated out of ODE at room temperature, it was used after preheating at 100 °C until it became transparent.

*Synthesis of the $CsPbBr_3$ Nanocrystals*: Briefly, 5 mL of *N*,*N*-dimethylformamide (DMF, Daejung, ≥99.5%) and 2.5 mmol $PbBr_2$ were loaded into a 10 mL flask. Subsequently, a combination of carboxylic acid and amine suitable for the synthesis of the perovskite nanocrystals, A*n*B*n*'-NCs, was added to the mixture. The types and amounts of suitable carboxylic acids and amines are detailed in Table S4, Supporting Information. The mixed solution was stirred until the $PbBr_2$ powder was completely dissolved and the solution was clear. After completely dissolving the $PbBr_2$, 0.165 mL of Cs-oleate (0.4 mol $L^{-1}$ in ODE) was added and dissolved in the mixed solution by stirring. Subsequently, 1 mL of the mixed solution was quickly injected into a 100 mL flask containing 30 mL toluene, after which the mixture was vigorously stirred at room temperature. The perovskite nanocrystals precipitated in the solution and the solution turned green. The perovskite nanocrystals, A*n*B*n*'-NCs, were allowed to react while stirring for a suitable reaction time. The appropriate reaction times are listed in Table S4, Supporting Information.

*Isolation and Purification of the $CsPbBr_3$ Nanocrystals*: The perovskite nanocrystals distributed in the crude solution were collected by centrifugation, followed by dispersion in hexane, whose volume was half that of the crude solution. Subsequently, ethyl acetate with the same volume as the hexane was then added to the hexane dispersion. The perovskite nanocrystals were collected again through centrifugation after washing, after which the nanocrystals were dispersed in hexane. Finally, washing and dispersing in hexane was performed once more.

*Characterizations*: FE-SEM images were obtained using a field-emission scanning electron microscope (Zeiss 300 VP) at an acceleration voltage of 10 kV. Transmission electron microscopy images were obtained using a transmission electron microscope (JEOL). The PL excitation and emission spectra were measured using a steady-state spectrofluorometer (PTI QuantaMaster) at an excitation wavelength of 365 nm. To measure PLQYs of the perovskite NCs, 100 nm integrating sphere (ILF-835) were equipped on the JASCO FP8500 spectrofluorometer. PLQY values were calculated by Jasco SpectraManager II Software. Powder XRD patterns were collected on a powder diffractometer (Bruker New D8-Advance) using monochromatized Cu K$\alpha$ radiation ($\lambda$ = 1.5418 Å). The UV–vis absorption spectra of the colloidal perovskite nanocrystals were collected using a spectrometer (JASCO, V-670) in transmission mode. The FT-IR spectra of the nanocrystals were collected using a Fourier-transform infrared spectrometer (Nicolet 6700).

## Supporting Information

Supporting Information is available from the Wiley Online Library or from the author.

## Acknowledgements

Y.-T.Y. and D.Y.H. contributed equally to this work. This research was supported in part by the Chung-Ang University Graduate Research Scholarship in 2018 and in part by the National Research Foundation of Korea (NRF) (2017M3D1A1039379, 2020R1A2C2100670).

 

## Conflict of Interest

The authors declare no conflict of interest.

## Data Availability Statement

The data that support the findings of this study are available from the corresponding authors upon reasonable request.

## Keywords

acid ligands, amine ligands, nanocrystals, perovskites, perovskite ligands

Received: January 18, 2021
Revised: March 27, 2021
Published online: April 21, 2021

[1] H. Huang, A. S. Susha, S. V. Kershaw, T. F. Hung, A. L. Rogach, *Adv. Sci.* **2015**, *2*, 1500194.
[2] H. Oga, A. Saeki, Y. Ogomi, S. Hayase, S. Seki, *J. Am. Chem. Soc.* **2014**, *136*, 13818.
[3] G. Nedelcu, L. Protesescu, S. Yakunin, M. I. Bodnarchuk, M. J. Grotevent, M. V. Kovalenko, *NanoLett.* **2015**, *15*, 5635.
[4] Q. A. Akkerman, V. D'Innocenzo, S. Accornero, A. Scarpellini, A. Petrozza, M. Prato, L. Manna, *J. Am. Chem. Soc.* **2015**, *137*, 10276.
[5] J. Kang, L.-W. Wang, *J. Phys. Chem. Lett.* **2017**, *8*, 489.
[6] L. C. Schmidt, A. Pertegás, S. González-Carrero, O. Malinkiewicz, S. Agouram, G. M. Espallargas, H. J. Bolink, R. E. Galian, J. Pérez-Prieto, *J. Am. Chem. Soc.* **2014**, *136*, 850.
[7] L. Protesescu, S. Yakunin, M. I. Bodnarchuk, F. Krieg, R. Caputo, C. H. Hendon, R. X. Yang, A. Walsh, M. V. Kovalenko, *Nano Lett.* **2015**, *15*, 3692.
[8] F. Zhang, H. Zhong, C. Chen, X. G. Wu, X. Hu, H. Huang, J. Han, B. Zou, Y. Dong, *ACS Nano* **2015**, *9*, 4533.
[9] D. N. Dirin, L. Protesescu, D. Trummer, I. V. Kochetygov, S. Yakunin, F. Krumeich, N. P. Stadie, M. V. Kovalenko, *Nano Lett.* **2016**, *16*, 5866.
[10] Z. Long, H. Ren, J. Sun, J. Ouyang, N. Na, *Chem. Commun.* **2017**, *53*, 9914.
[11] Q. Pan, H. Hu, Y. Zou, M. Chen, L. Wu, D. Yang, X. Yuan, J. Fan, B. Sun, Q. Zhang, *J. Mater. Chem. C* **2017**, *5*, 10947.
[12] H. Huang, Q. Xue, B. Chen, Y. Xiong, J. Schneider, C. Zhi, H. Zhong, A. L. Rogach, *Angew. Chem., Int. Ed.* **2017**, *56*, 9571.
[13] Y. Tong, E. Bladt, M. F. Aygüler, A. Manzi, K. Z. Milowska, V. A. Hintermayr, P. Docampo, S. Bals, A. S. Urban, L. Polavarapu, *Angew. Chem., Int. Ed.* **2016**, *5*, 13887.
[14] V. A. Hintermayr, A. F. Richter, F. Ehrat, M. Döblinger, W. Vanderlinden, J. A. Sichert, Y. Tong, L. Polavarapu, J. Feldmann, A. S. Urban, *Adv. Mater.* **2016**, *28*, 9478.
[15] Z. Y. Zhu, Q. Q. Yang, L. F. Gao, L. Zhang, A. Y. Shi, C. L. Sun, Q. Wang, H. L. Zhang, *J. Phys. Chem. Lett.* **2017**, *8*, 1610.
[16] S. Bai, W. Wu, Y. Qin, N. Cui, D. J. Bayerl, X. Wang, *Adv. Funct. Mater.* **2011**, *21*, 4464.
[17] W. Zhang, L. Peng, J. Liu, A. Tang, J. S. Hu, J. Yao, Y. S. Zhao, *Adv. Mater.* **2016**, *28*, 4040.
[18] H. Lin, C. Zhou, Y. Tian, T. Siegrist, B. Ma, *ACS Energy Lett.* **2017**, *3*, 54.
[19] H. Zheng, G. Liu, L. Zhu, J. Ye, X. Zhang, A. Alsaedi, T. Hayat, X. Pan, S. Dai, *Adv. Energy Mater.* **2018**, *8*, 1800051.
[20] G. Jia, Z. J. Shi, Y. D. Xia, Q. Wei, Y. H. Chen, G. C. Xing, W. Huang, *Opt. Express* **2018**, *26*, A66.
[21] E. R. Dohner, A. Jaffe, L. R. Bradshaw, H. I. Karunadasa, *J. Am. Chem. Soc.* **2014**, *136*, 13154.
[22] E. R. Dohner, E. T. Hoke, H. I. Karunadasa, *J. Am. Chem. Soc.* **2014**, *136*, 1718.
[23] L. Mao, Y. Wu, C. C. Stoumpos, M. R. Wasielewski, M. G. Kanatzidis, *J. Am. Chem. Soc.* **2017**, *139*, 5210.
[24] Y. Yin, A. P. Alivisatos, *Nature* **2005**, *437*, 664.
[25] C. R. Bealing, W. J. Baumgardner, J. J. Choi, T. Hanrath, R. G. Hennig, *ACS Nano* **2012**, *6*, 2118.
[26] S. Sun, D. Yuan, Y. Xu, A. Wang, Z. Deng, *ACS Nano* **2016**, *10*, 3648.
[27] A. Pan, B. He, X. Fan, Z. Liu, J. J. Urban, A. P. Alivisatos, L. He, Y. Liu, *ACS Nano* **2016**, *10*, 7943.
[28] Z. Yuan, Y. Shu, Y. Xin, B. Ma, *Chem. Commun.* **2016**, *52*, 3887.
[29] X. Yang, X. Zhang, J. Deng, Z. Chu, Q. Jiang, J. Meng, P. Wang, L. Zhang, Z. Yin, J. You, *Nat. Commun.* **2018**, *9*, 570.
[30] Y. F. Ng, S. A. Kulkarni, S. Parida, N. F. Jamaludin, N. Yantara, A. Bruno, C. Soci, S. Mhaisalkar, N. Mathews, *Chem. Commun.* **2017**, *53*, 12004.
[31] Y. H. Kim, C. Wolf, Y. T. Kim, H. Cho, W. Kwon, S. Do, A. Sadhanala, C. G. Park, S. W. Rhee, S. H. Im, *ACS Nano* **2017**, *11*, 6586.
[32] J. De Roo, M. Ibáñez, P. Geiregat, G. Nedelcu, W. Walravens, J. Maes, J. C. Martins, I. V. Driessche, M. V. Kovalenko, Z. Hens, *ACS Nano* **2016**, *10*, 2071.

 